Dielectronic recombination and resonant transfer excitation processes for helium-like krypton*

Hu Xiao-Li(胡骁骊)[a], Qu Yi-Zhi(屈一至)[a]†, Zhang Song-Bin(张松斌)[b], and Zhang Yu(张 宇)[c]

[a] *College of Material Sciences and Optoelectronic Technology, Graduate University of the Chinese Academy of Sciences, P. O. Box* 4588, *Beijing* 100049, *China*

[b] *Department of Chemistry, Texas A & M University, College Station, TX* 77842, *USA*

[c] *The Key Laboratory of Computational Physics, Institute of Applied Physics and Computational Mathematics, P. O. Box* 8009, *Beijing* 100088, *China*

(Received 9 March 2012; revised manuscript received 12 April 2012)

The relativistic configuration interaction method is employed to calculate the dielectronic recombination (DR) cross sections of helium-like krypton via the $1s2lnl'$ ($n = 2, 3, \ldots, 15$) resonances. Then, the resonant transfer excitation (RTE) processes of Kr^{34+} colliding with H, He, H_2, and CH_x (x = 0–4) targets are investigated under the impulse approximation. The needed Compton profiles of targets are obtained from the Hartree–Fock wave functions. The RTE cross sections are strongly dependent on DR resonant energies and strengths, and the electron momentum distributions of the target. For H_2 and H targets, the ratio of their RTE cross sections changes from 1.85 for the $1s2l2l'$ to 1.88 for other resonances, which demonstrates the weak molecular effects on the Compton profiles of H_2. For CH_x (x = 0–4) targets, the main contribution to the RTE cross section comes from the carbon atom since carbon carries 6 electrons; as the number of hydrogen increases in CH_x, the RTE cross section almost increases by the same value, displaying the strong separate atom character for the hydrogen. However, further comparison of the individual orbital contributions of C(2p, 2s, 1s) and $CH_4(1t_2, 2a_1, 1a_1)$ to the RTE cross sections shows that the molecular effects induce differences of about 25.1%, 19.9%, and 0.2% between $2p$–$1t_2$, $2s$–$2a_1$, and $1s$–$1a_1$ orbitals, respectively.

Keywords: dielectronic recombination, Compton profile, resonant transfer excitation

PACS: 34.50.Fa, 34.80.Dp **DOI:** 10.1088/1674-1056/21/10/103401

1. Introduction

Dielectronic recombination (DR) is an important atomic process which affects the ionization balance and radiation energy in high-temperature plasmas produced in the laboratory or in astrophysics.[1] DR can be regarded as a two-step process. First, a free electron with a certain energy is captured by an ion, forming a doubly excited intermediate state. This intermediate state can then decay into a nonautoionizing state by emitting a stabilizing photon. Similar to the DR process, the resonant transfer excitation (RTE) process in collisions of highly charged ions with atoms or molecules can also be regarded as a two-step process, but the ion captures a binding electron in the atom or molecule target instead of a free electron. Therefore, one can test the theoretical model for the RTE process and obtain information about the momentum distribution of bounded electrons in the target atoms or molecules. In recent years, there has been a lot of work[2–6] related to the RTE process and the theoretical results are in general agreement with the experimental results. However, the Compton profiles of atoms and molecules in the previous reports[5,6] are obtained from experimental measurements, and detailed studies on the RTE cross sections for various targets are scarce.

In the present work, we perform a detailed theoretical study of RTE processes for helium-like krypton with H, He, H_2, and CH_x (x = 0–4) targets since krypton has been proposed as a coolant of future tokamak[1] and H, He, H_2, and CH_x (x = 0–4) are often the components in the plasma edge or the divertor of a tokamak.[7] The required Compton profiles are obtained from the wave functions calculated by the Hatree–Fock method with different basis sets 6-31G,[8] cc-pVTZ,[9–11] and cc-pVQZ.[9–11] The Compton profiles are found to be sensitive to the choice of basis

*Project supported by the National Natural Science Foundation of China (Grant Nos. 1179041, 11025417, and 10979007) and the NSAF (Grant No. 10876043).

†Corresponding author. E-mail: yzqu@gucas.ac.cn

© 2012 Chinese Physical Society and IOP Publishing Ltd

functions in the small momentum region. The DR cross sections for Kr^{34+} ion are calculated by using the Flexible Atomic Code (FAC)[12−14] with the relativistic configuration interaction method, which has been successfully used to calculate the DR cross sections and rate coefficients of Ne-like Au ions.[15] Our DR results accord well with other calculations.[16] Then, the RTE cross sections in collisions of Kr^{34+} ions with H, He, H_2, and CH_x (x = 0–4) targets are investigated for the first time, and the dependence of the RTE cross section on target is analysed.

The rest of this paper is organized as follows. In Section 2 we briefly outline the theoretical method used in calculations of the Compton profile and the DR and RTE cross sections. The results and discussions are given in Section 3. Our conclusions are presented in Section 4.

2. Theoretical approach

2.1. Dielectronic recombination

For the ground state of helium-like krypton, the DR process has the form

$$\begin{aligned} \mathrm{Kr}^{34+}(1\mathrm{s}^2)_i + \mathrm{e}^- &\rightarrow \mathrm{Kr}^{33+}(1\mathrm{s}2l n l')_j^{**} \\ &\rightarrow \mathrm{Kr}^{33+}(1\mathrm{s}^2 n''\mathrm{l}'')_k + h\nu, \quad (1) \end{aligned}$$

where Kr^{34+} ion in the initial state $i(1s^2)$ captures a free electron with a specific energy ε_{ij}, and forms a Kr^{33+} ion in the resonant doubly excited state $j(1s2lnl')^{**}$. The DR strength, which is the integration of the DR cross sections on incident electron energies, can be written in the isolated resonance approximation as[5]

$$S_{ij,k} = \frac{\pi^2\hbar^3}{(m_\mathrm{e}\varepsilon_{ij})}\frac{g_j}{2g_i}A^a_{ji}\frac{A^r_{jk}}{\sum\limits_{k'}A^r_{jk'}+\sum\limits_{i'}A^a_{ji'}}, \quad (2)$$

where m_e is the electron mass, g_i and g_j are the statistical weights of initial state i and the doubly excited intermediate state j, respectively. $\sum\limits_{k'}A^r_{jk'}$ and $\sum\limits_{i'}A^a_{ji'}$ are the total radiative and Auger rates of state j, respectively. The FAC is employed to calculate the energy levels, Auger and radiative transition rates, in which the relativistic configuration interaction approximation is used to calculate the bound–bound transition processes and the autoionization processes are treated in the first-order perturbation theory using distorted-wave approximation for the continuum electrons.[16]

2.2. Resonant transfer excitation

Similar to the DR process, the RTE process of helium-like krypton can be written as

$$\begin{aligned} \mathrm{Kr}^{34+}(1\mathrm{s}^2) + B &\rightarrow \mathrm{Kr}^{33+}(1\mathrm{s}2l n l')^{**} + B^+ \\ &\rightarrow \mathrm{Kr}^{33+}(1\mathrm{s}^2 n''\mathrm{l}'') + B^+ + h\nu', \quad (3) \end{aligned}$$

where B represents the target atom or molecule. The weakly bounded electrons of the target B are analogous to the free electron in the DR process. When the velocity of projectile ion is much larger than the orbital velocity of the target electron and the distortion of the projectile resonance state by the target nucleus is small, the impulse approximation[17] can be employed to calculate the RTE cross section for a fixed projectile state i. The RTE cross section has the form

$$\sigma_\mathrm{RTE} = \sum_{j,k} S_{ij,k} J(q) \left[\frac{M}{2E}\right]^{1/2}, \quad (4)$$

where M is the mass of the projectile, E is the projectile energy in the laboratory frame, and $J(q)$ is the Compton profile of the target electron.

2.3. Compton profile

For an atom, the Compton profile can be obtained by integrating the momentum distribution probability of the target electron as[18]

$$J(q) = 2\pi\int_{|q|}^{\infty} pn(p)\mathrm{d}p, \quad (5)$$

$$n(p) = |\psi(p)|^2, \quad (6)$$

where p is the magnitude of the electron momentum; $\psi(p)$ can be obtained through Fourier transmation in polar coordinate as[19]

$$\begin{aligned} \psi(p) = &\int_0^\infty\int_0^\pi\int_0^{2\pi} \mathrm{e}^{-(2\pi\mathrm{i}/h)pr\cos\theta} \\ &\times\phi(r)r^2\sin\theta\mathrm{d}r\mathrm{d}\theta\mathrm{d}\varphi; \quad (7) \end{aligned}$$

q is the momentum of target electron which can be deduced by the energy conservation law as[5]

$$q = \left(E_j + E_\mathrm{t} - \frac{m_\mathrm{e}}{M}E\right)\left(\frac{M}{2E}\right)^{1/2}. \quad (8)$$

Here E_j is the energy of the intermediate doubly excited state and E_t is the binding energy of the target electron. E_t can be ignored in Eq. (8) since it is very small in comparison to the value of $(E_j - m_\mathrm{e}E/M)$. Then equation (8) can be reduced to

$$q = \left(E_j - \frac{m_\mathrm{e}}{M}E\right)\left(\frac{M}{2E}\right)^{1/2}. \quad (9)$$

As for a randomly oriented molecule, $n(p)$ should be replaced by the orientation averaged momentum distribution probability $\overline{n(p)}$, which can be approximated with the electron momentum spectra of the relevant molecular orbital $\sigma_{\rm EMS}$ and expressed as

$$\overline{n(p)} \approx \sigma_{\rm EMS} = C \int {\rm d}\Omega \, |\psi(\boldsymbol{p})|^2, \qquad (10)$$

where $\psi(\boldsymbol{p})$ is the electron wave function in the momentum space of one electron momentum $\boldsymbol{p} = (p_x, p_y, p_z)$, C is a kinematic term which is constant if symmetric non-coplanar scattering geometry is used,[20] and it could be determined by the normalization of the Compton profile

$$\int_{-\infty}^{\infty} J(q) {\rm d}q = 1 \quad \text{for each electron.} \qquad (11)$$

For atoms and molecules which have multiple orbitals, the measurement of Compton profiles involves both summation of individual orbitals as well as integration over the momentum distributions.[21]

3. Results and discussion

3.1. DR cross sections

The DR strengths of helium-like krypton ions via the $1s2lnl'$ ($n = 2, 3, \ldots, 15$) resonances calculated by the FAC are given in Table 1 and compared with the results of Biedermann *et al.*[22] using the HULLAC code. The deviations between the two results are less than 5%.

Table 1. DR strengths of Kr^{34+} for KLL ($1s2l2l'$), KLM ($1s2l3l'$), KLN ($1s2l4l'$), and KLO ($1s2l5l'$) resonances (10^{-20} cm^2·eV).

Resonance	KLL	KLM	KLN	KLO
HULLAC[21]	54.2	30.4	12.3	6.1
This work	55.9	31.1	12.7	6.4

The DR cross section can be obtained from the DR strength convoluted with the Gaussian distribution of the incident energy resolution $\Delta\varepsilon$[14] as

$$\sigma_{ij}(\varepsilon) = S_{ij}^{\rm DR} \frac{2}{\Delta\varepsilon} \sqrt{\frac{\ln 2}{\pi}} \exp\left(-4 \ln 2 \frac{(\varepsilon - \varepsilon_{ij})^2}{\Delta\varepsilon^2} \right). \qquad (12)$$

In Fig. 1, the DR cross sections in an incident energy region of 8.5 keV–13.5 keV are plotted with $\Delta\varepsilon = 50$ eV, the same as that in Ref. [16]. It can be seen that our results are in good agreement with the results calculated by FAC in Ref. [16].

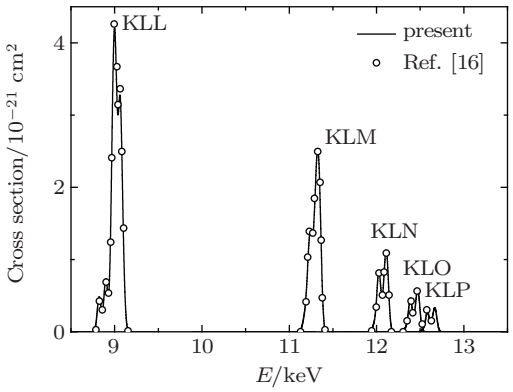


Fig. 1. DR cross sections for Kr^{34+} in an energy region of 8.5 keV–13.5 keV.

3.2. Compton profile

To obtain the Compton profiles of He and H_2, we first calculate the wave functions by the Hatree–Fock method. The basis 6-31G, cc-pVTZ, and cc-pVQZ are adopted to check the convergence. The internuclear separation of H_2 is set to be 1.4 a.u. (atomic units). Our calculation results are compared with experimental ones,[18,23–25] as shown in Figs. 2(a) and 2(b).

It can be seen that as the electron momentum q increases, the Compton profiles of both H_2 and He decline to zero as $q \to \infty$. This can be understood by the integral relation of Eq. (5). In the large momentum region, the differences between Compton profiles calculated from different basis sets are small. However, there are obvious differences in the small momentum region between 6-31G and cc-pVTZ/cc-pVQZ basis, which means that the calculations of wave functions in 6-31G basis without the polarized functions are not accurate. In the whole momentum region, the Compton profiles based on cc-pVTZ and cc-pVQZ differ from each other slightly. Thus, it can be concluded that the cc-pVQZ basis is large enough to obtain accurate Compton profiles of H_2 and He, which will be used in the RTE calculations.

The Compton profiles of H, H_2, and He are compared in Fig. 2(c). It is easy to find that the Compton profile of H_2 is less than twice the Compton profile of H, because of the interaction between two hydrogen atoms in the hydrogen molecule. On the other hand, although both H_2 and He have two electrons, their Compton profiles are quite different. When $q \leq 0.61$ a.u., the Compton profile of H_2 is greater than that of He. And for $q \geq 0.61$ a.u., the situation is reversed, which is also reported in earlier experimental work.[25] It indicates the difference between the atomic wave function and molecular wave function for the isoelectronic system. For H and He atoms, the Compton

profile of He becomes larger as the number of electrons in atoms increases since the Compton profile reflects the electron momentum distribution.

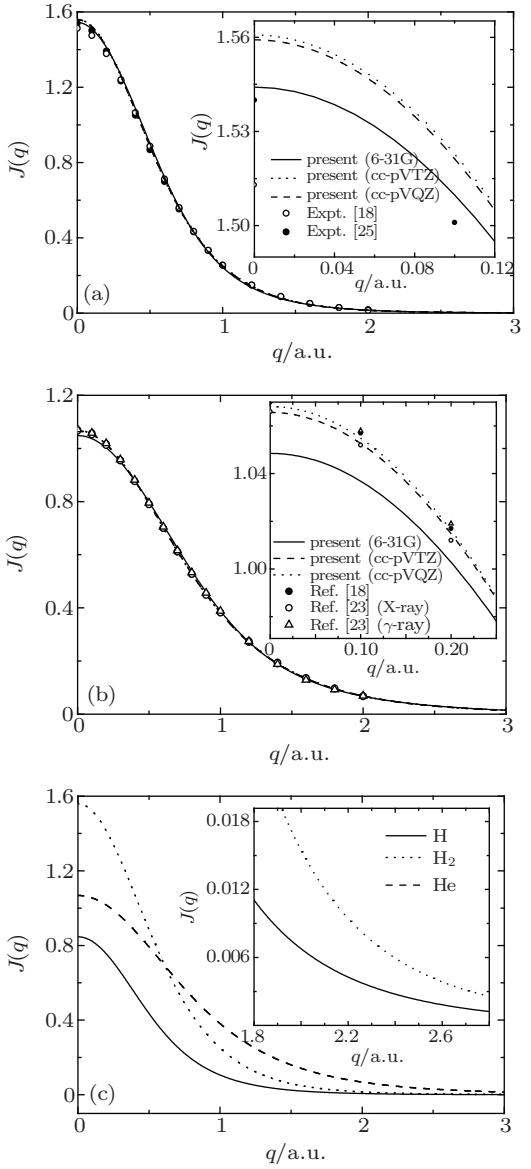


Fig. 2. Compton profiles of H_2 (a) and He (b) under different basis sets, and the comparison of Compton profiles of H, H_2, and He with the basis of cc-pVQZ (c).

In Table 2, we give the bond lengths of CH_x (x = 1–4), which are obtained from the optimization calculation of GAUSSIAN 98[26] in the cc-pVQZ basis. We use point group symmetry C_v for CH, C_{2v} for CH_2, C_{3v} for CH_3, and T_d for CH_4. Comparison with NIST data[27] shows that our calculations are reliable.

Table 2. The C–H bond lengths of CH, CH_2, CH_3, and CH_4 (bond length is in 10^{-10} m).

Level/Basis set	CH (C_v)	CH_2 (C_{2v})	CH_3 (C_{3v})	CH_4 (T_d)
B3LYP/cc-pVQZ	1.122	1.109	1.077	1.087
NIST[27]	1.120	1.085	1.079	1.087

The Compton profiles of H and CH_x (x = 0–4) are plotted in Fig. 3(a) for comparison. One can find that the Compton profiles of CH_x (x = 0–4) are quite similar in line shape, and they increase as x increases. However the increased value is less than that of the Compton profile of H in the small momentum region because of the binding interaction of molecules. When the electron momentum $q \geq 2$ a.u., the Compton profiles of CH_x (x = 0–4) are very close, since the Compton profile of H approaches to zero in the large momentum region.

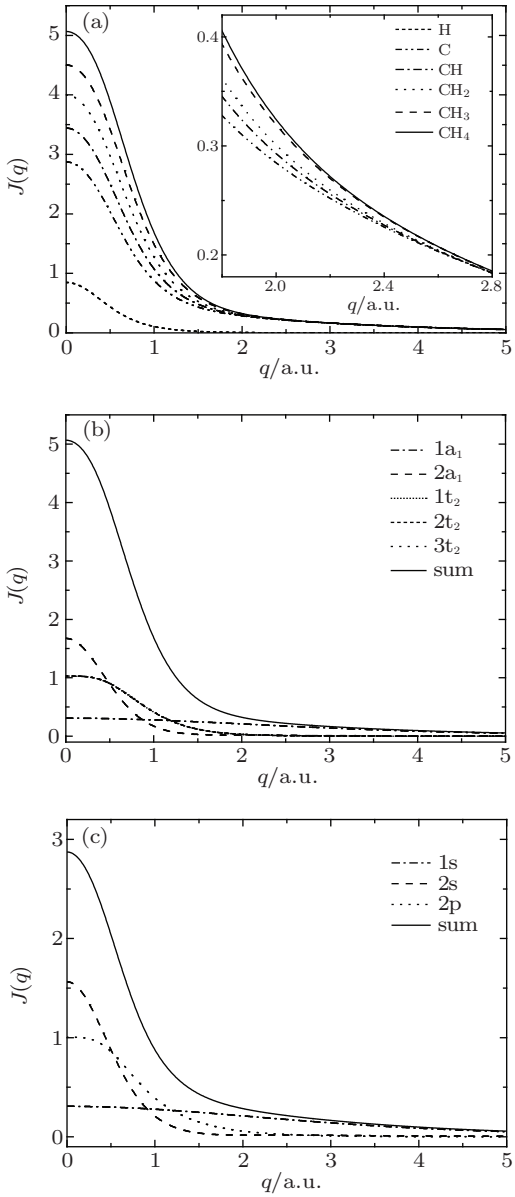


Fig. 3. (a) Comparison of Compton profiles among H and CH_x (x = 0–4); (b) Compton profiles of individual orbitals of CH_4; (c) the Compton profiles of individual orbitals of C.

In order to investigate the molecular effect on the orbital electrons, we examine the Compton profiles

of individual orbitals of CH_4 with ground state electron configuration $(1a_1)^2(2a_1)^2(1t_2)^2(2t_2)^2(3t_2)^2$ and C with $1s^22s^22p^2$ as shown in Figs. 3(b) and 3(c), respectively. The ionization energy of each individual orbital is summarized in Table 3, and there exist obvious differences between 2p–$1t_2$ and 2s–$2a_1$ orbitals. The Compton profiles of $1t_2$, $2t_2$, $3t_2$ are in full coincidence in Fig. 3(b). In a small electron momentum region ($q < 1.2$ a.u.), the $1t_2$, $2t_2$, and $3t_2$ contribute to the major part of the total Compton profile. When the electron momentum is greater than 1.2 a.u., the $1a_1$ contribution dominates. Then, at a large electron momentum ($q > 3$ a.u.), the total Compton profile of CH_4 is contributed mainly by the Compton profile of the orbital $1a_1$ and the contributions of other orbitals are near zero. This is because the outer orbital in the coordinate space corresponds to small momentum in the momentum space, and the inner orbital corresponds to large momentum. It is consistent with the energy order in our calculation. For $1t_2$, $2t_2$, and $3t_2$, they are degenerate in energy. Detailed analysis of the molecular orbitals with GAUSSIAN98[25] shows that the $1a_1$, $2a_1$, $1t_2$, $2t_2$, and $3t_2$ molecular orbitals in CH_4 are mainly composed of 1s, 2s, $2p_x$, $2p_y$, $2p_z$ orbitals of carbon. Therefore, it is easy to understand that the Compton profiles of CH, CH_2, CH_3, and CH_4 are quite similar to that of C.

Table 3. Ionization energies of the individual orbitals of CH_4 and C (in units of eV).

Orbitals of CH_4	$1a_1$	$2a_1$	$1t_2$	$2t_2$	$3t_2$
Ionization energy	304.8	25.6	14.8	14.8	14.8
Orbitals of C	1s	2s	2p		
Ionization energy	309.1	19.7	9.7		

3.3. RTE cross sections

Using the DR strengths and Compton profiles, the RTE cross sections via $1s2lnl'$ ($n = 2, 3, \ldots, 15$) resonances can be obtained. Figure 4 shows the RTE cross section as a function of projectile energy for Kr^{34+} in colliding with H, H_2, and He targets, respectively. For the Kr^{34+} + H and Kr^{34+} + H_2 collisions, the first maximum values occurring at 1.38×10^9 eV are 6.60×10^{-22} cm^2 and 12.22×10^{-22} cm^2, respectively, and it mainly comes from the contribution of doubly excited state $1s2l2l'$. The peak position is determined by the resonance energy and the magnitude relies on both the DR strength and Compton profile. The second maximum values occurring at 1.73×10^9 eV are 3.55×10^{-22} cm^2 and 6.69×10^{-22} cm^2, which come from the contribution of $1s2lnl'$ ($n \geq 3$) resonances. The ratios of the first peak and the second peak for the two collision systems are 1.85 and 1.88, deviating from 2, which results from the H_2 target molecular effect. Similarly, the first maximum value of 8.49×10^{-22} cm^2 occurs at 1.38×10^9 eV for the Kr^{34+} + He collision, and the second maximum value of 5.33×10^{-22} cm^2 appears at 1.75×10^9 eV. Obviously, the difference in RTE cross section between Kr^{34+} + H_2 and Kr^{34+} + He is mostly due to the difference in Compton profile between H_2 and He although they are isoelectronic systems. From Fig. 2(c), it can be noted that the Compton profile of He is broader than that of H_2, which leads to a shoulder on the right side of the second peak of Kr^{34+} + H_2 RTE cross section. Therefore, the RTE cross sections display the electron momentum distribution of target electrons.

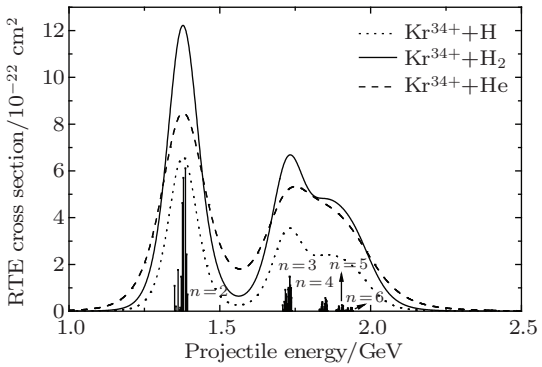


Fig. 4. RTE cross sections for Kr^{34+} + H, H_2, and He collision processes. (The vertical bars indicate the theoretical positions and relative heights of the DR strengths, the notation $n = 2, 3, 4$ etc. refers the principal quantum numbers of the intermediate doubly excited states $1s2lnl'$).

Figure 5(a) gives the RTE cross sections from the individual 1s, 2s, and 2p orbitals of carbon. For comparison, the RTE cross sections from the $1a_1$, $2a_1$, and $1t_2$ orbitals of CH_4 are also displayed in Fig. 5(b). Because the individual orbital of CH_4 is partly composed of the individual orbitals of carbon, it can be expected that the RTE cross sections for CH_4($1a_1$, $2a_1$, $1t_2$) are similar to those of C(1s, 2s, 2p). Interestingly, the RTE cross sections for both Kr^{34+} + C(1s) and Kr^{34+} + CH_4($1a_1$) have only one peak around the projectile energy 1.52×10^9 eV, because the Compton profiles of CH_4($1a_1$) and C(1s) extend to a broad range of more than 5 a.u., where no evident peak exists, and the RTE peak is contributed by all doubly excited states $1s2l2l'$, $1s2l3l'$, and $1s2l4l'$. The magnitudes of RTE peaks for Kr^{34+} + C(1s) and Kr^{34+} + CH_4($1a_1$) are 3.431×10^{-22} cm^2 and

3.432×10^{-22} cm^2, respectively, which indicates the atomic character. For the Kr^{34+} + C(2s) and Kr^{34+} + $CH_4(2a_1)$ collisions, the first maximum values occurring at 1.37×10^9 eV are 12.32×10^{-22} cm^2 and 13.14×10^{-22} cm^2 , respectively; the second maximum values appearing at 1.73×10^9 eV are 6.69×10^{-22} cm^2 and 7.02×10^{-22} cm^2 , respectively. Besides, the RTE cross section for Kr^{34+} + C(2p) has two major peaks: one peak of 8.05×10^{-22} cm^2 at 1.37×10^9 eV and the other peak of 5.45×10^{-22} cm^2 at 1.77×10^9 eV; similarly, for the Kr^{34+} + $CH_4(1t_2)$ collision, the two peaks of 8.25×10^{-22} cm^2 and 5.63×10^{-22} cm^2 occur at 1.37×10^9 eV and 1.77×10^9 eV, respectively. For the projectile energy between 1×10^9 eV and 3×10^9 eV, the average RTE cross sections for Kr^{34+} + $CH_4(1t_2)$, Kr^{34+} + $CH_4(2a_1)$, and Kr^{34+} + $CH_4(1a_1)$ change by 25.1%, 19.9%, 0.2% compared with those of Kr^{34+} + C(2p), Kr^{34+} + C(2s), and Kr^{34+} + C(1s), respectively. The obvious differences in magnitude between $CH_4(2a_1)$ and C(2s) and between $CH_4(1t_2)$ and C(2p) imply the differences between atomic and molecular orbitals. It also could be found that the second peak of Kr^{34+} + C(2p) is on the right side of the second peak of Kr^{34+} + C(2s), which indicates that the contribution of doubly excited state 1s2l4l′ is larger than that of 1s2l3l′ in Kr^{34+} + C(2p).

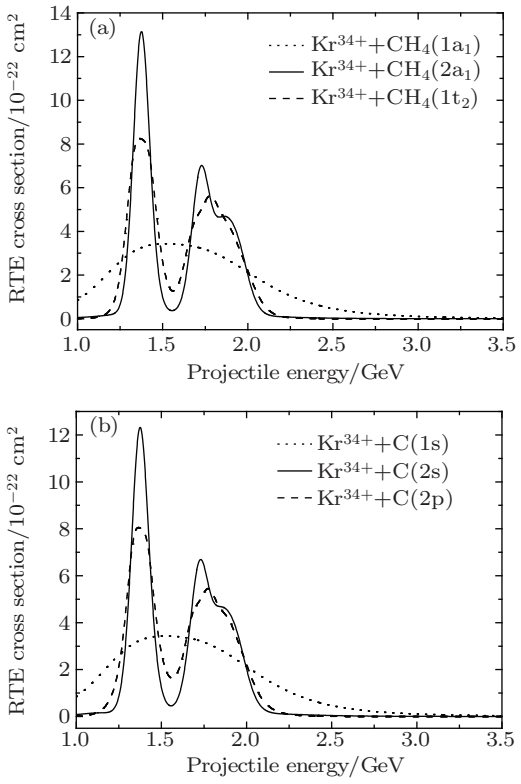


Fig. 5. RTE cross sections for individual orbitals of (a) Kr^{34+} + CH_4 and (b) Kr^{34+} + C.

The total RTE cross sections for the helium-like krypton with H and CH_x (x = 0–4) are plotted in Fig. 6. Because of the similarity of the shapes of Compton profiles for CH_x (x = 0–4), the RTE cross sections of Kr^{34+} + CH_x (x = 0–4) are also quite similar. When the number of H atoms increases, the RTE cross sections also increase, but the positions of the two major peaks at 1.37×10^9 eV and 1.73×10^9 eV contributed by the 1s2l2l′ and 1s2l3l′ ($n \geq 3$) resonances, respectively, are independent of the number of H atoms. We also note that as the value of x increases in the RTE processes of Kr^{34+} + CH_x (x = 0–4), the shoulder on the right side of the second peak begins to disappear because of the broader Compton profile of CH_x with the value of x increasing.

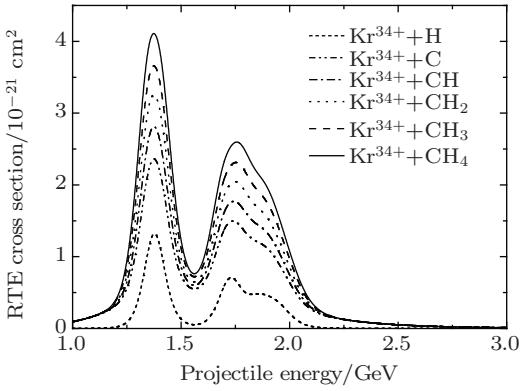


Fig. 6. RTE cross sections for Kr^{34+} + H, C, CH, CH_2, CH_3, CH_4 (RTE cross sections for Kr^{34+} + H has been multiplied by a factor of 2).

4. Conclusion

Based on the relativistic configuration interaction method, the dielectronic recombination cross sections of helium-like krypton via 1s2lnl' ($n = 2, 3, \ldots, 15$) resonances are calculated using the FAC. Then, the RTE processes for Kr^{34+} with H, He, H_2, and CH_x (x = 0–4) targets are investigated in the impulse approximation for the first time. The required Compton profiles are obtained from the Hatree–Fock wave functions calculated by using the GAUSSIAN98 package. Usually, the RTE cross section has some resonant structures, and the position of peak is strongly dependent on the resonance energies of the doubly excited states and the magnitude of peak relies on both the DR strength and Compton profiles of targets. Therefore, the RTE cross section can reflect the electron momentum distribution in the target. Compared with the atomic and molecular targets, it can be found that the RTE cross section from the inner orbitals is weakly

dependent on the molecular character; however, the RTE cross section from the outer orbitals can be easily influenced including the peak position and magnitude. Further experiments are expected to test the present theoretical results of Compton profiles and RTE cross sections.

References

[1] Fuchs T, Biedermann C, Radtke R, Behar E and Doron R 1998 *Phys. Rev.* A **58** 4518

[2] Tanis J A, Bernstein E M, Clark M W, Graham W G, McFarland R H, Morgan T J, Mowat J R, Mueller D W, Muller A, Stockli M P, Berkner K H, Gohil P, McDonald R J, Schlachter A S and Sterns J W 1986 *Phys. Rev.* A **34** 2543

[3] Tanis J A, Bernstein E M, Graham W G, Stockli M P, Clark M, McFarland R H, Morgan T J, Berkner K H, Schlachter A S and Sterns J W 1984 *Phys. Rev. Lett.* **53** 2551

[4] Ma X, Mokler P H, Bosch F, Gumberidze A, Kozhuharov C, Liesen D, Sierpowski D, Stachura Z, Stohlker Th and Warczak A 2003 *Phys. Rev.* A **68** 042712

[5] Dong C Z and Fu Y B 2006 *Acta Phys. Sin.* **55** 107 (in Chinese)

[6] Dong C Z, Wang J G, Qu Y Z and Li J M 1999 *Phys. Scr.* **T80** 301

[7] Nakano T, Kubo H, Higashijima S, Asakura N, Takenaga H, Sugie T and Itami K 2002 *Nucl. Fusion* **42** 689

[8] Hehre W J, Ditchfield R and People J A 1972 *J. Chem. Phys.* **56** 2257

[9] Dunning T H Jr 1989 *J. Chem. Phys.* **90** 1007

[10] Woon D E and Dunning T H Jr 1994 *J. Chem. Phys.* **100** 2975

[11] Kendall R A and Dunning T H Jr 1992 *J. Chem. Phys.* **96** 6796

[12] Gu M F 2003 *Astrophys. J.* **582** 1241

[13] Gu M F 2003 *Astrophys. J.* **589** 1085

[14] Gu M F 2003 *Astrophys. J.* **590** 1131

[15] Liu X J, Qu Y Z, Xiao B J and Wang J G 2009 *Eur. Phys. J.* D **55** 57

[16] Shi X H, Wang Y S, Chen C Y and Gu M F 2005 *Chin. Phys.* **14** 959

[17] Brandt D 1983 *Phys. Rev.* A **27** 1314

[18] Eisenberger P 1970 *Phys. Rev.* A **2** 1678

[19] Dumond J W M 1929 *Phys. Rev.* **33** 643

[20] Brion C E, Cooper G, Zheng Y, Litvinyuk I V and McCarthy I E 2001 *Chem. Phys.* **270** 13

[21] Dey S, McCarthy I E, Teubner P J O and Weigold E 1975 *Phys. Rev. Lett.* **34** 782

[22] Biedermann C, Fuchs T, Liebisch P, Radtke R, Behar E and Doron R 1999 *Phys. Scr.* **T80** 303

[23] Eisenberger P and Reed W A 1972 *Phys. Rev.* A **5** 2085

[24] Jeziorski B and Szalewicz K 1979 *Phys. Rev.* A **19** 2360

[25] Lee J S 1976 *J. Chem. Phys.* **66** 4906

[26] Frisch M J, Trucks G W, Schlegel H B, Gill P M W, Johnson B G, Robb M A, Cheeseman M J R, Keith T A, Petersson G A, Montgomery J A, Raghavachari K, Al-Laham M A, Zakrzewski V G, Ortiz J V, Foresman J B, Ciosloswki J, Stefanof B B, Nanayakkara A, Challacombe M, Peng C Y, Ayala P Y, Chen W, Wong M W, Andres J L, Replogle E S, Gomperts R, Martin R L, Fox D J, Binkley J S, Defrees D J, Baker J, Stewart J P, Head–Gordon M, Gonzalez C and Pople J A 1998 *Gaussian* 98 Revision **A.9**

[27] Linstrom, P J and Mallard, W G 2001 *NIST Chemistry WebBook, NIST Standard Reference Database* **No. 69** (Gaithersburg: National Institute of Standards and Technology, http://webbook.nist.gov.)